Journal of Industrial and Engineering Chemistry 108 (2022) 195–202

Contents lists available at ScienceDirect

Journal of Industrial and Engineering Chemistry

journal homepage: www.elsevier.com/locate/jiec

Trace surface fluorination and tungsten-intercalation cooperated dual modification induced photo-activity enhancement of titanium dioxide

Yifan Xu [a,d,1], Zhongyuan Liu [a,1], Kunlun Wang [a], Chunyao Niu [b,*], Pengfei Yuan [b], Jin You Zheng [c], Young Soo Kang [d], Xiao Li Zhang [a,*]

[a] School of Materials Science and Engineering, Zhengzhou University, 450001 PR China
[b] School of Physics and Microelectronics, Zhengzhou University, 450001 PR China
[c] School of Chemical Engineering, Zhengzhou University, Zhengzhou 450001, China
[d] Department of Chemistry, Sogang University, Seoul 121–742, Republic of Korea

ARTICLE INFO

Article history:
Received 12 October 2021
Revised 24 December 2021
Accepted 28 December 2021
Available online 4 January 2022

Keywords:
TiO_2
Dual modification
Tungsten doping
Surface fluorination
Density functional calculation

ABSTRACT

General modification that utilizes insoluble tungstic acid or highly toxic hydrofluoric acid to improve charge separation and transfer in TiO_2 results in considerable issues such as uneven doping, significant impacts on particle size and morphology, as well as environmental hazards. In the present work, an environmental benign one-pot dual-modification approach was demonstrated that uses soluble sodium tungstate and only trace-level sodium fluoride as replacements. The photoactivity efficiency for decoloration of methylene blue (MB) solution was improved by 33.6% and 119.5% under ultraviolet and visible light, respectively. Meanwhile, the photocurrent density reached an enhancement by 181.2% by this dual-modification. The dual-modification had negligible influence on the crystal structure and the surface area of the TiO_2 nanoparticles. Density functional calculation suggested the remarkable improvements of the photocatalysis of TiO_2 can be ascribed to the rapid charge separation and transfer owing to the down-shift of conduction band from the tungsten doping and localized spatial charge separation from the surface fluorination enabled by the dual-modification approach.

Introduction

Possessing the ability to enable chemical reactions through utilizing the most abundant free energy – sun light, photocatalysis is one of the most promising and feasible technologies in advanced oxidation processes. Since Fujima and Honda's pioneering work on water splitting using TiO_2, low cost, earth-abundance, non-toxicity and high resistance to corrosion/photocorrosion have made titanium dioxide an excellent candidate for environmental and sustainable applications [1–4]. Significant efforts have been dedicated to explore its potential on scientific and technological applications through a broad range of material design, synthesis and engineering strategies.

Transition metal doping is a proven practical modification technique to widen the absorption of TiO_2 from ultraviolet range to visible range while retard the recombination of photogenerated charges and facilitate rapid interfacial charge transfer. In comparison to other transition metal dopants, such as chromium (III, 75.5 pm), vanadium (III, 78 pm), nickel (II, 83 pm), magnesium (II, 72 pm) and iron (II, 78 pm; III, 69 pm) [5,6], the tungsten (VI, 74 pm) has the closest radius to that of the titanium (IV, 74.5 pm), which would form stable doping in the lattice of the titanium dioxide. Studies have shown that doping tungsten enabled red shift of light absorption and prompts efficient charge transfer [7].

Separately, as the photocatalytic reaction mainly occurs on the catalyst surface [8], surface modification also greatly influence the adsorption and reaction rate. Fluorination has become one of the most effective ways for surface acidification due to the strong electronegativity of the fluorine [9]. The ≡Ti-F group transfers electrons to the O atoms on the surface of the fluorinated TiO_2 to capture photoelectrons [10–16]. However, the low boiling point volatile and seriously toxic HF [17,18] may release highly noxious vapor that violates the original purpose aiming at environmental sustainability [19]. Environmental benign alternative methods are, therefore, greatly desired for delivering comparable performances.

* Corresponding authors.
E-mail address: xiaolizhang.z@gmail.com (X.L. Zhang).
[1] The authors contributed equally to this work.

https://doi.org/10.1016/j.jiec.2021.12.035
1226-086X/

In the present work, in contrast, a feasible environmental friendly one-pot dual functional synthesis strategy were successfully developed that utilized water-soluble sodium tungstate and only trace-amount of sodium fluoride. This would ease the preparation and prevent inhomogeneity of the products and significantly reduce the environmental impacts of the chemical wastes from the material preparation process [19,20]. Combined characteristic analyses and density functional calculation suggested that the noteworthy enhancements on the ultraviolet light and visible light photoactivities can be ascribed to rapid charge separation and transfer as a result of the bandgap narrowing from tungsten doping and a localized spatial charge separation induced by surface F-adsorption.

Experiment

Materials synthesis

All chemicals used in the present work were from Sinopharme Chemical Reagent Co. Ltd including Degussa P25 titanium dioxide, sodium hydroxide, hydrochloric acid 32 %, sodium tungstate dihydrate, sodium fluoride and methylene blue. All the chemicals are of reagent grade. Water was obtained from a milli-Q integral water purification system of 18.2 mΩ/cm resistivity.

The synthesis process was schematically illustrated in the Scheme 1. In a typical synthesis of the precursor, 0.5 g of P25 was initially dispersed into 30 ml of water with vigorous stirring, then 6 g of sodium hydroxide was added to form a 5 M aqueous NaOH solution. After another 10 min of constant stirring, the solution was transferred into a 50 ml Teflon liner autoclave. The autoclave was sealed before heated in an oven at 140 °C for 10 h. After cooling to the room-temperature, the obtained white sodium titanate was transferred out from the autoclave and washed 3 times with 500 mL of water before washing with 500 mL of 0.1 M HCl solution. The resulted hydrogen titanate was collected by centrifugation.

To prepare the tungsten doped and/or fluorinated TiO_2 nanoparticles, the collected white precursor was re-dispersed into 30 mL of water with stoichiometric sodium tungstate (with a ratio of W:Ti of 0.5%, 0.75% and 1%) and transferred into 50 ml Teflon liner autoclave. The modification such as W-doping, Fluorination and dual-modification processes was implemented with a hydrothermal treatment at 180 °C for another 10 h. For fluorinated samples, sodium fluoride with a ratio for F:Ti of 10^{-6}:1 was added into the 30 mL precursor slurry before the hydrothermal treatment.

Following the hydrothermal process, the obtained nanoparticle was separated by centrifugation, then was washed 3 times with water before drying at 60 °C in a drying oven overnight. Prior to photocatalytic activity tests, all the samples were calcined at 450 °C for 30 min in a muffle furnace. The samples were labeled following the tungsten doping level and fluorination such as pure TiO_2, 0.5% W, 0.75% W, 1.0% W, FT and FT-1.0% W.

Characterization

PANalytical Xpert Multipurpose X-ray Diffraction System was used for XRD analysis. TEM images were obtained by Phillips CM200 transmission electron microscope. Specific surface area of the prepared products were analysed using Micromeritics TriStar 3000. Solid phase UV–Vis analysis was measured on a Shimadzu UV-3600 UV–Vis-NIR spectrophotometer whereas solution phase UV–Vis analysis was performed using Cary 3000 Scan UV–visible spectrophotometer.

Photocatalytic MB decoloration

40 mL of photocatalyst suspension with a solid concentration of 0.5 g/L and 0.20 mL of methylene blue solution (1.10 g/L) were premixed in a glass bottle covered with aluminium foil to prevent from exposure to light. The glass bottle was left on a roller mixer (Ratek SP354) for a continuous mixing of 20 min to reach an adsorption – desorption equilibrium ahead of the illumination using 3 × 18 W of ultraviolet light (UV) or fluorescent light (VL) as light sources. 4.0 mL of the sample was collected every 10 minutes to analyse the remaining MB by a UV-spectrophotometer. Throughout all the experiments, the suspension was kept constant rolling and mixing on the roller mixer.

Photoelectrochemical measurement

The electrochemical measurement uses Shanghai Chenhua CHI 760E electrochemical workstation. The electrochemical test was performed with a standard three electrode system (Glassy carbon electrode is the working electrode, Ag/AgCl electrode is the reference electrode, Pt electrode is the counter electrode). 5 mg of the synthesized sample was dispersed in a mixed solution of 1 mL deionized water 500 μL of isopropanol, and 50 μL of Nafion. The mixture was sonicated for 30 minutes in a sonication bath before coating on glassy carbon electrodes. 10 μL of prepared uniform suspension was dropped on the glassy carbon electrodes and then dried in the oven. 50 mL of 0.5 M Na_2SO_4 solution was prepared as electrolyte solution. Photocurrent stability and response were studied by measuring the photocurrent produced at +0.5 V vs Ag/AgCl under 300 W Xe lamp illumination. Electrochemical impedance spectroscopy (EIS) was conducted using a potentiostat. The frequency was set from 0.01 Hz to 1000 kHz at 0.5 V vs Ag/AgCl and the amplitude was 0.05 V.

Computational simulation detail

First-Principle calculations were implemented within the framework of density functional theory with the spin-polarization being considered [21]. The projector-augmented wave (PAW) approach [22,23] and the generalized gradient approximation (GGA) [24] for the exchange–correlation energy functional were carried out in the Vienna ab initio simulation package (VASP) [25–27]. The GGA calculation was implemented using the Perdew-Burke-Ernzerhof (PBE) [28] exchange–correlation potential. The (101) surface was chosen as the main surface in the following computational simulation according to the XRD analysis with (101) facet is the exposed surface. The anatase (101) surface was modeled with a (2 × 3) four-Ti-layer slab (48 Ti and 96 O atoms) with a vacuum thickness of 16 Å. A plane-wave cutoff energy of 450 eV was applied. The Brillouin-zone was sampled with a 3 × 3 × 1 Monkhorst-Pack. All atoms were completely relaxed of a tolerance in total energy of 0.1 meV, while the forces on each atom were no more than 0.03 eV/Å. The vdW interaction is treated using the DFT-D3 method proposed by Grimme [29]. The experimental bulk lattice parameters (a = 3.786 Å, c = 9.514 Å) of TiO_2 are used for the (101) surface calculations throughout the present work. To produce electronic structure properties more accurately, the DFT + U method was used, where the onsite Coulomb correction was set on Ti 3d orbitals with an effective U value of 4.2 eV as suggested in literature works [30,31]. The tetrahedron method (ISMEAR = −5) was used to produce the accurate density of states and fermi level positions of the systems.

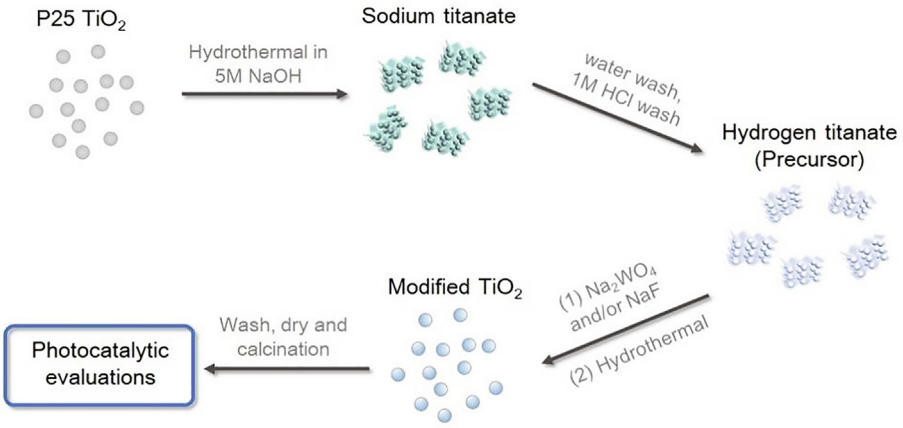

Scheme 1. Schematic illustration of the synthesis process for W, F and dual-modified TiO_2.

Results and discussions

Transmission electron microscopy (TEM) observation was utilized to estimate the influences from tungsten doping and trace-level fluorination on the morphology and distribution of particle size for the obtained TiO_2 nanoparticles. High-resolution TEM and overall TEM images of TiO_2 nanoparticles with different tungsten doping and fluorination levels are shown in Fig. 1 and insets. Fig. 1a-c) represent an increased tungsten doping level from 0, 0.5 to 1%, respectively. The particles are of irregular shape with clear edges indicating a well-developed crystalline structure [32]. All samples are of similar main size distribution of approximately 10–30 nm suggesting a minor influence on the particle size from the tungsten doping. In Fig. 1a-c) insets, the corresponding lattice fringes are of 0.35 nm that can be assigned to the (101) planes of anatase TiO_2. The distinct and sharp lattice fringes in Fig. 1a-b) suggest negligible effect on the crystalline development at a low doping level of 0.5%, while surface defects can be easily observed when the doping level reached 1% in Fig. 1c). Fig. 1d-e) are the trace-level fluorinated TiO_2 that also exhibit insignificant impact on the size, morphology and crystalline structure of the TiO_2 nanoparticles with and without tungsten doping at different doping levels.

XRD patterns of the W-doped and fluorinated TiO_2 nanoparticles are shown in Fig. 2a) and b), respectively. All of XRD characteristic peaks can be well assigned to anatase-phased TiO_2 (tetragonal, JCPD card No. 21-1272) and rutile-phased TiO_2 (JCPD card No. 21-1276) [33–36] in a phase ratio of approximately 85:15 similar to that of the commercial Degussa P25 TiO_2 nanoparticles [37]. All the samples have similar values for the average grain size of approximately 25–30 nm that were estimated from the Scheele equation using the full width at half maximum (FWHM) of the peak (101) at 25.3° which are in consistence with the TEM observations [33,34,38,39]. The XRD analyses further confirm negligible changes on the development of the crystalline structure of the TiO_2 nanoparticles from the modifications including W-doping, trace-level fluorination and dual modification at current specific solvothermal reactions.

Nitrogen gas sorption analysis utilizing the Barrett-Joyner-Halenda (BJH) method was conducted to evaluate the specific surface area of the tungsten and fluorine modified TiO_2 samples. The corresponding Brunauer-Emmett-Teller (BET) analyses results were exhibited in Fig. 2c), d) and Table 1. All samples exhibited similar shapes of typical IV isotherms [19,39] with H1 type hysteresis loops corresponding to the mesoporous texture with minor alteration of the specific surface areas from the tungsten doping and/or the fluorination [40]. As summarized in the Table 1, W-doping, fluorination and dual-modification only exhibited negligible effects on the specific surface area of the particles with values from 39 m^2/g to approximately 42–47 m^2/g, which is consistent with the aforementioned TEM and XRD analyses.

XPS spectra evaluated the chemical composition and bonding states for the elements of the W-doped TiO_2 nanoparticles (W-TiO_2) and dual-modified TiO_2 nanoparticles (FW-TiO_2), as shown in Fig. 3. Fig. 3a) reveals main peak of 458.6 eV and 464.6 eV that

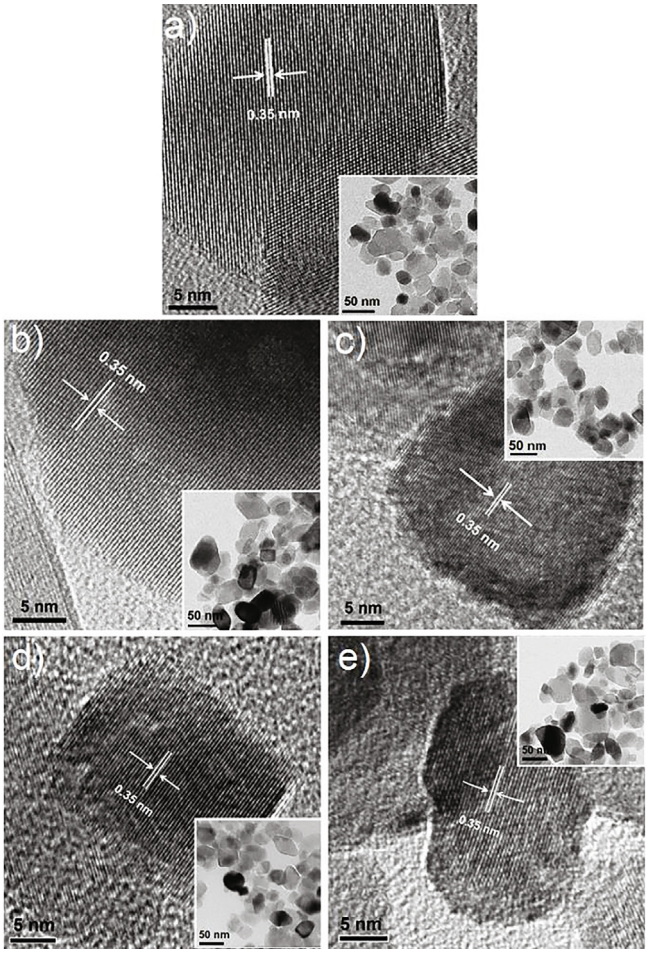

Fig. 1. TEM images of TiO_2 nanoparticles synthesized without and with tungsten doping and fluorination: a) pure TiO_2, b) 0.5%W, c) 1.0%W, d) FT and e) FT-1.0%W.

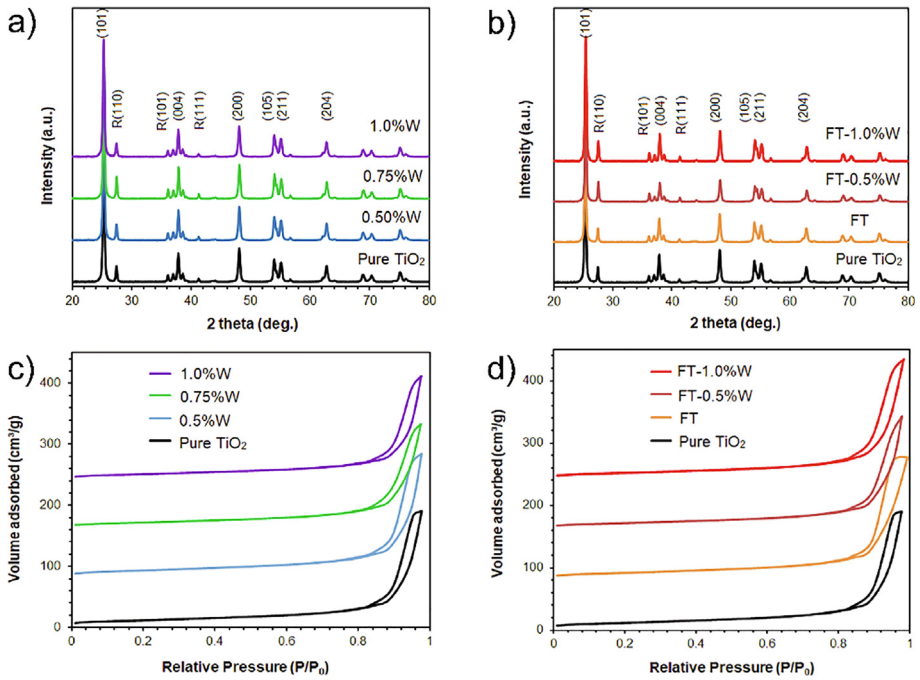

Fig. 2. a-b) XRD and c-d) nitrogen adsorption isotherms of as-synthesized TiO_2 nanoparticles with a) and c) varying W-doping levels; b) and d) surface fluorination.

can be ascribed to Ti^{4+} $2p_{3/2}$ and Ti^{4+} $2p_{1/2}$, respectively, with small peaks of Ti^{3+} were also observed at 463.8 eV. A broad peak ranging from 31.8 eV to 41.6 eV in Fig. 3b) can be attributed to the Ti3p and the W4f, while the peaks at 35.48 eV and 37.58 eV can be ascribed to $4f_{7/2}$ and $4f_{7/5}$ of W, respectively. The binding energy difference of 2.1 eV matches to the horizontal splitting of W4f [40]. The peak at 37.08 eV is from Ti3p level. Fig. 3c) exhibits the peaks at 241.0 eV to 243.3 eV that can be assigned to the W4d. These suggest the existence of W in TiO_2. As shown in Fig. 3d), the FW-TiO_2 has a F1s binding energy of 684 eV corresponding to the fluorination of TiO_2 due to physical adsorption of F^- on the surface of TiO_2 crystals [41]. Comparison of the W-TiO_2 and FW-TiO_2, XPS results suggest that such physical adsorption induced fluorination has negligible effect on the electronic state of Ti and W.

Typical photocatalytic decoloration of dye-methylene blue (MB) under ultraviolet light (UV) and visible light (VL) illumination was employed to demonstrate the influence from W-doping, surface fluorination and dual-modification on the chemical properties of the TiO_2 nanoparticles. Fig. 4a) and b) exhibit the comparison studies of the photocatalytic decoloration under UV irradiation using the W-doped, surface fluorinated and dual-modified TiO_2 to evaluate the consequent effects. The photocatalytic decoloration curves have a rapid drop in the first 3 min then a moderated decoloration under the UV irradiation. The photocatalytic decoloration performances of all samples are well beyond that of the non-modified TiO_2, as shown in the Fig. 4a). The results show that the decoloration performance of presented W-doped TiO_2 was enhanced with the increasing W-doping level. In comparison with the pure TiO_2, the photodegradation rates of the samples with 0.5%, 0.75% and 1% tungsten doping increased by approximately 5.5%, 19.8% and 26.1%, respectively. The increasing of photocatalysis activity is possibly due to the development of new band near the conduction band minimum (CBM) of TiO_2 from the W-doping that efficiently facilitates the photogenerated electron transfer and charge separation [42,43]. In Fig. 4b), the surface fluorination enabled an enhancement by approximately 5.0% and a further 5.9% for the TiO_2 and the 1.0% W-doped TiO_2, respectively, while the dual-modification led to a total 33.6% improvement compared to that of the un-modified TiO_2. Based on the aforementioned XPS analysis, the strong electronegativity of the F adsorbed on TiO_2 surface [43] might facilitate the charge trapping and transport leading to the activity enhancements.

Fig. 4c) shows visible light irradiated decoloration using W-doped, surface fluorinated and dual-modified TiO_2 with commercial Degussa P25 TiO_2 as a reference material. The pure TiO_2, P25 and FT (fluorinated TiO_2) give linear decoloration curves while the W-doped samples present a rapid decoloration at the first 3 min following with moderated steady decoloration rates. In comparison to the pure TiO_2 and P25, surface fluorination exhibited an improved decoloration efficiency by 50.3% and 9.9%, respectively. While the dual modified sample (FT-1%W) achieved decoloration enhancements by 119.5% and 60.5% against the pure TiO_2 and P25, respectively, with an almost steady excellent performance during the following testing. The results show that both tungsten doping and fluorination have noteworthy impacts on the photocatalytic performance of TiO_2 nanoparticles, while the dual-modification demonstrated superior enhancement on the photocatalytic activity, especially for the activity at the visible light range. The photocatalytic performance of the FT-1%W sample was also compared with other fluorinated or W-modified TiO_2 photocatalysts reported in the literature in Table 2.

Photoelectric test was conducted on the synthesized samples with the corresponding experimental results are exhibited in Fig. 5. In contrast to the un-modified TiO_2, both tungsten doping and surface fluorination significantly enhanced the photocurrent

Table 1
Specific surface area of as-synthesized TiO_2 nanoparticles with varying W-doping levels and surface fluorination.

Sample	Surface Area (m^2/g)
Pure TiO_2	41.8
0.50%W	47.4
0.75%W	41.9
1.0%W	39.0
FT	42.0
FT-0.5%W	41.5
FT-1.0%W	42.4

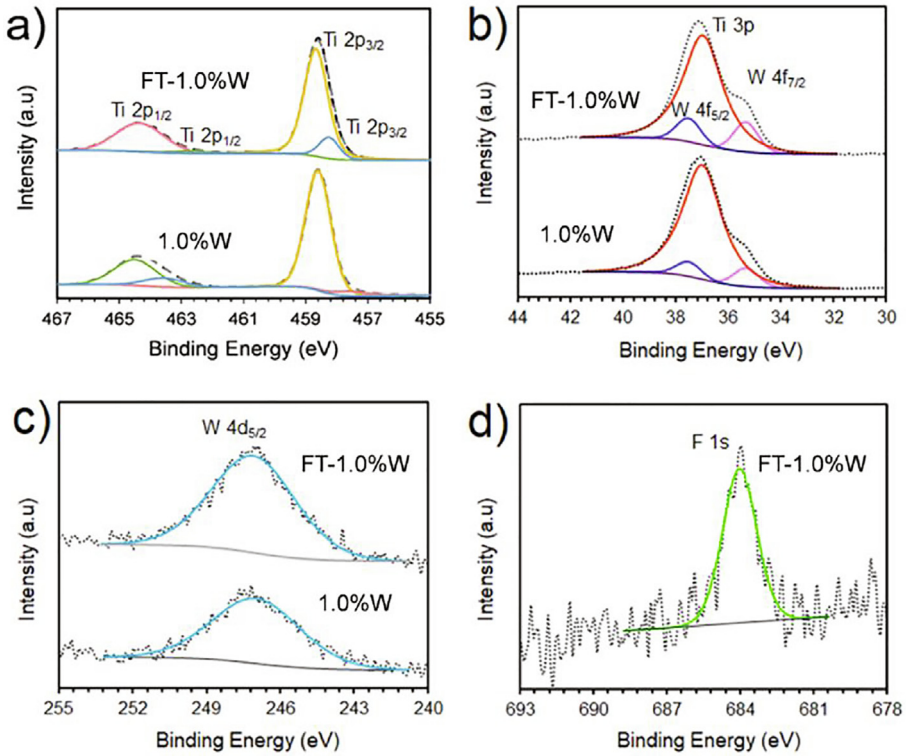

Fig. 3. XPS spectra of sample FT-1.0%W and 1.0%W: a) Binding energy peaks of Ti; b) and c) The signal and fittings corresponding with the typical signals of W binding energy; d) Binding energy of F.

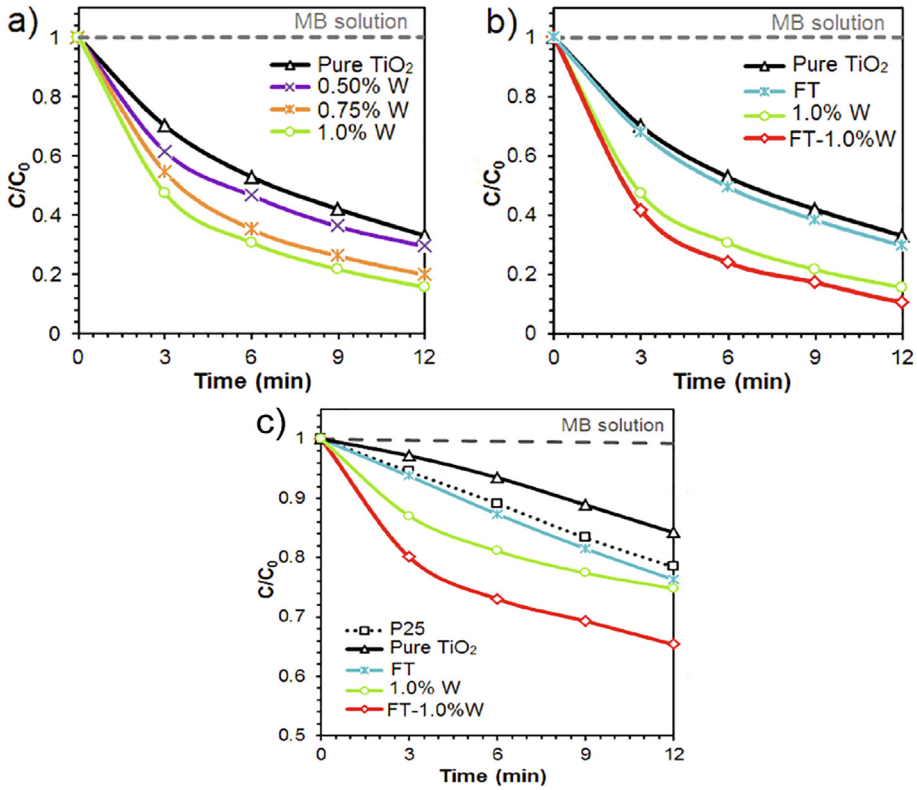

Fig. 4. Photocatalytic decoloration of MB under UV light using TiO_2 nanoparticles with a) varying doping levels and b) surface fluorination; c) under visible light using TiO_2 nanoparticles with varying doping levels and surface fluorination.

Table 2
Degradation efficiency of organics for TiO_2-based Photocatalysts from the literature[49–55]

Photocatalyst	Light	Organic pollutants	Degradation (%)	Degradation time (min)	Reference
W/F-TiO_2	UV	MB	90	12	this work
	VL		34		
F-TiO_2	UV	MB	90	40	19
	VL		16		
WO_3-TiO_2	UV	Malachite Green	85	120	49
	VL		67		
F_2-TiO_2	UV	MB	73	240	50
1%F/10%Si-TiO_2	UV	MO	99	60	51
W/F-TiO_2	VL	MB	90	150	52
WO_3-TiO_2 film	UV	MO	40	150	53
N/F-TiO_2	VL	MB	97.3	300	54
F-TiO_2	VL	Atrazine	43.2	180	55

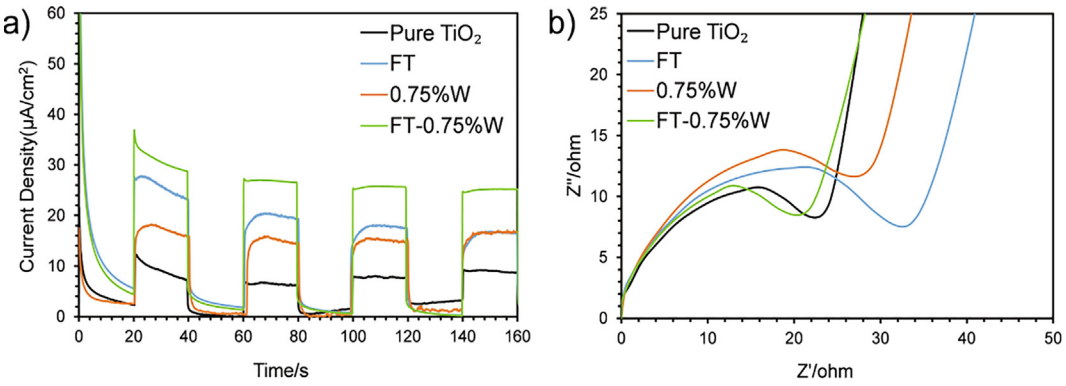

Fig. 5. a) Photocurrent test and b) impedance test of TiO_2 nanoparticles with varying tungsten doping levels and surface fluorination under visible light.

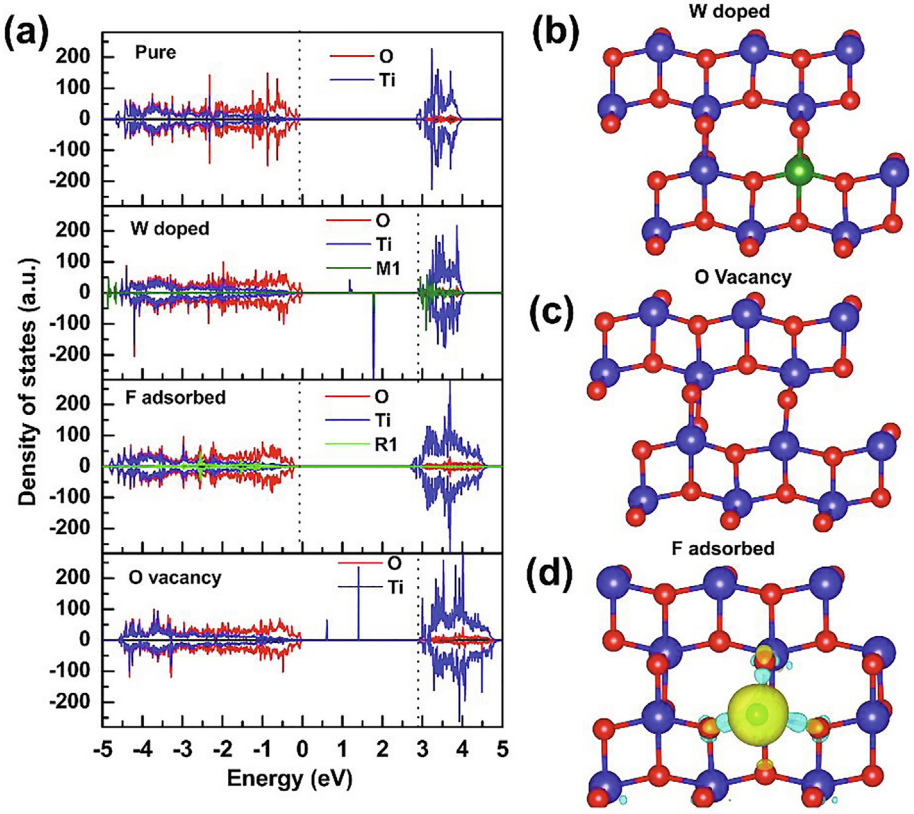

Fig. 6. a) The density of states for pure, W-doped, F-adsorbed and O vacancy of TiO_2 (101) surface. The values of F and W are multiplied by five. The dotted line is the Fermi level. b) and c) Structures of the TiO_2 (101) surface with W doped and O vacancy, respectively. d) The charge density difference of the fluorine adsorbed TiO_2 surface.

density of the TiO_2 nanoparticles. At the first 20 seconds, the 0.75% W-doped TiO_2 reached a current density of 18 $\mu A/cm^2$, of surface fluorination enabled a current density of 28 $\mu A/cm^2$ of the TiO_2 and dual-modified TiO_2 achieved 35.9 $\mu A/cm^2$ while the un-modified TiO_2 only reached 10 $\mu A/cm^2$. In the first 120 seconds, in contrast to un-modified TiO_2, the 0.75% tungsten-doped and the surface fluorinated sample show a certain attenuation on the photocurrent density with an enhancement by averagely 108.3% and 175.2%, respectively. The photocurrent density of the two samples stabilized at approximately 16.63$\mu A/cm^2$ with nearly 85.4% higher than that of the un-modified TiO_2. The dual-modification resulted the highest photocurrent density over 30 $\mu A/cm^2$ at the beginning and stabile value of about 25.22 $\mu A/cm^2$ after 140 seconds with only a slight attenuation, which exhibits an enhancement by approximately 181.2% compared to the un-modified TiO_2. Fig. 5b) shows the impedance test results of TiO_2 nanoparticles. The curve radius of the dual-modified TiO_2 is similar to that of pure TiO_2. The surface fluorinated samples showed the largest curve radius, followed by samples doped with 0.75% W suggesting that the electron conductivity in TiO_2 was improved with decrease of recombination rate of the electron/hole pairs from the W-doping and fluorination which would attribute to the photoactivity.

Aiming at a better understanding of these phenomena, first-principle calculations within density function theory (DFT) calculations were performed to investigate the electronic structures of the TiO_2 (101) surface, surface with W-doped, F-adsorbed, and O-vacancy, as shown in the Fig. 6. According to the XRD results, the predominated (101) surface of TiO_2 was chosen as the main surface in the following computational simulation with (101). The band gap for the pure TiO_2 (101) is 3.0 eV that agrees well with the previous literature [44,45]. The simulation results suggest that the three types of defects in this work do not have significant influence on the band gap. However, W-doping or O-vacancy induces new band states which corresponds to the formation of Ti^{3+}. These Ti^{3+} gap states can reduce the recombination of the electron and hole effectively and thus enhances photocatalytic activity. In case of F-adsorbed surface, there is no gap states observed in band gap. The F states are fully occupied and involved in the middle of the VBM demonstrating the shift of electron from the TiO_2 towards the fluorine atoms. As exhibited in Fig. 6d), in case of the F atom adsorbed on the top of Ti atoms, the charge variation involves charge drifting away from the Ti atoms and accumulating around F atoms which result in a localized spatial charge separation. This would significantly benefit rapid polarization of the excited charge carriers immediately after the generation during the photocatalysis. Owing to the strong electronegativity, the electrons would transfer to the F atoms and thus retard the recombination and significantly prompt the photoactivity performances [19,46–48]. As a result, the narrowed band gap caused by tungsten doping and the local electric fields induced by F adsorption enabled the greatly improved photocatalytic activity in this work.

Conclusion

In summary, an environmental benign and simple one-pot dual modification process that utilize soluble sodium tungstate and trace-level sodium fluoride as alternative modification regents has been successfully developed. The tungsten and fluoride dual-modification has very minor impact on the crystalline structure and the specific surface area of the TiO_2 particles. In addition, tungsten doping successfully narrowed the bandgap and surface fluoride adsorption enabled a localized spatial charges separation, thereby promoting the rapid separation and transfer of charges during photocatalysis. This significantly prompted the photocatalytic activity of the TiO_2 nanoparticles that includes 33.6% and 119.5% enhancements on the photocatalytic decoloration efficiency of methylene blue (MB) under ultraviolet and visible light, respectively, and an increase on the photocurrent density of 181.2%.

Declaration of Competing Interest

The authors declare that they have no known competing financial interests or personal relationships that could have appeared to influence the work reported in this paper.

Acknowledgement

X.L.Z. would like to thank the funding support from the National Natural Science Foundation of China (NSFC, Grant No.: 51602291).

References

[1] L.X. Zheng, F. Teng, X.Y. Ye, H.J. Zheng, X.S. Fang, Adv. Energy Mater. 10 (2020) 1902355.
[2] P. Niu, T.T. Wu, L. Wen, J. Tan, Y.Q. Yang, S.J. Zheng, et al., Adv. Mater. 30 (2018) 1705999.
[3] Z.L. Tian, P.F. Zhang, P. Qin, D. Sun, S.N. Zhang, X.W. Guo, et al., Adv. Energy Mater. 9 (2019) 1901287.
[4] Y. Yang, L. Cui, B. Wang, R. Qiao, D. Chen, J. Fan, et al., ChemPhotoChem 2 (2018) 986–993.
[5] Q.Q. Yin, R. Qiao, Z.Q. Li, X.L. Zhang, L.L. Zhu, J. Alloy. Compd. 618 (2015) 318–325.
[6] T.Z. Huang, S. Mao, J.M. Yu, Z.H. Wen, G.H. Lu, J.H. Chen, RSC Adv. 3 (2013) 16657–16664.
[7] V. Štengl, J. Velická, M. Maříková, T.M. Grygar, ACS Appl. Mater. Inter. 3 (2011) 4014–4023.
[8] A.L. Linsebigler, G.Q. Lu, J.T. Yates, Chem. Rev. 95 (1995) 735–758.
[9] A.Y. Meng, J. Zhang, D.F. Xu, B. Cheng, J.G. Yu, Appl. Catal. B-Environ. 198 (2016) 286–294.
[10] Y.R. Yang, K. Ye, D.X. Cao, P. Gao, M. Qiu, L. Liu, et al., Mater. Inter. 10 (2018) 19633–19638.
[11] J.W. Chen, G.X. Wu, T.Y. Wang, X.D. Li, M.C. Li, Y.H. Sang, et al., Mater. Inter. 9 (2017) 4634–4642.
[12] S. Ghosh, L. Manna, Chem. Rev. 118 (2018) 7804–7864.
[13] J.L. Long, H.J. Chang, Q. Gu, J. Xu, L.Z. Fan, S.C. Wang, et al., Energ. Environ. Sci. 7 (2014) 973–977.
[14] X.S. Zhou, F. Peng, H.J. Wang, H. Yu, Y.P. Fang, Chem. Commun. 48 (2012) 600–602.
[15] Y. Yang, Y. Liang, G.Z. Wang, L.L. Liu, C. Yuan, T. Yu, et al., Mater. Inter. 7 (2015) 24902–24908.
[16] J. Zhang, S. Chen, L.S. Qian, X. Tao, L.X. Yang, H.B. Wang, et al., J. Am. Ceram. Soc. 97 (2014) 4005–4010.
[17] H.G. Yang, C.H. Sun, S.Z. Qiao, J. Zou, G. Liu, S.C. Smith, et al., Nature 453 (2008) 638–641.
[18] National Center for Biotechnology Information. PubChem Database. Hydrofluoric acid, CID = 14917; https://pubchem.ncbi.nlm.nih.gov/compound/Hydrofluoric-acid.
[19] Y. Xu, T.F. Tay, L. Cui, J. Fan, C. Niu, D. Chen, et al., Inorg. Chem. 59 (2020) 17631–17637.
[20] E.M. Neville, M.J. Mattle, D. Loughrey, B. Rajesh, M. Rahman, J.M.D. MacElroy, et al., J. Phys. Chem. C 116 (2012) 16511–16521.
[21] W. Kohn, L.J. Sham, Phys. Rev. 140 (1965) 1133–1138.
[22] P.E. Blöchl, Phys. Rev. B: Condens. Matter Mater. Phys. 50 (1994) 17953–17979.
[23] G. Kresse, D. Joubert, Phys. Rev. B: Condens. Matter Mater. Phys. 59 (1999) 1758–1775.
[24] J.P. Perdew, Y. Wang, Phys. Rev. B: Condens. Matter Mater. Phys. 45 (1992) 13244–13249.
[25] G. Kresse, J. Hafner, Phys. Rev. B: Condens. Matter Mater. Phys. 47 (1993) 558–561.
[26] G. Kresse, J. Furthmüller, Phys. Rev. B: Condens. Matter Mater. Phys. 54 (1996) 11169–11186.
[27] G. Kresse, J. Furthmüller, Comp. Mate. Sci. 6 (1996) 15–50.
[28] J.P. Perdew, K. Burke, M. Ernzerhof, Phys. Rev. Lett. 77 (1996) 3865–3868.
[29] S. Grimme, J. Antony, S. Ehrlich, H. Krieg, J. Chem. Phys. 132 (2010) 154104.
[30] B.J. Morgan, G.W. Watson, Surf. Sci. 601 (2007) 5034–5041.
[31] L.K. Yan, H.N. Chen, J. Chem. Theory Comput. 10 (2014) 4995–5001.
[32] K.P.S. Parmar, E. Ramasamy, J.W. Lee, J.S. Lee, Scripta Mater. 62 (2010) 223–226.
[33] S.Y. Wang, M.T. Soe, K.T. Guo, X.L. Zhang, Z.X. Guo, RSC Adv. 5 (2015) 41059–41065.
[34] D. Chen, F. Huang, Y.-B. Cheng, R.A. Caruso, Adv. Mater. 21 (2009) 2206–2210.
[35] X.L. Zhang, W. Huang, A. Gu, W. Xiang, F. Huang, Z.X. Guo, et al., J. Mate. Chem. C 5 (2017) 4875–4883.

[36] Y.M. Lei, J. Li, Z. Wang, J. Sun, F. Chen, H.W. Liu, et al., Nanoscale 9 (2017) 4601–4609.
[37] Y. Liu, H.Q. Wang, Z.B. Wu, J. Environ. Sci. 19 (2007) 1505–1509.
[38] L. Cao, D. Chen, R.A. Caruso, Angew. Chem. Int. Ed. 52 (2013) 10986–10991.
[39] L. Cui, Y. Xu, J. Fan, P. Yuan, C. Sun, Z.X. Guo, et al., Energ. Mater. 4 (2021) 4050–4058.
[40] K.S.W. Sing, Pure Appl. Chem. 54 (1982) 2201–2218.
[41] J.C. Yu, J.G. Yu, W. Ho, Z.T. Jiang, L.Z. Zhang, Chem. Mater. 14 (2002) 3808–3816.
[42] X. Zhang, F. Liu, Q.L. Huang, G. Zhou, Z.S. Wang, J. Phys. Chem. C 115 (2011) 12665–12671.
[43] A.M. Cant, F. Huang, X.L. Zhang, Y. Chen, Y.-B. Cheng, R. Amal, Nanoscale 6 (2014) 3875–3880.
[44] F.F. Sanches, G. Mallia, L. Liborio, U. Diebold, N.M. Harrison, Phys. Rev. B 89 (2014) 245309.
[45] G. Mattioli, F. Filippone, P. Alippi, A. Amore Bonapasta, Phys. Rev. B 78 (2008) 241201(R).
[46] L. Hao, L. Kang, H.W. Huang, L.Q. Ye, K.L. Han, S.Q. Yang, et al., Adv. Mater. 31 (2019) 1900546.
[47] C.Y. Mao, F. Zuo, Y. Hou, X.H. Bu, P.Y. Feng, Angew. Chem., Int. Ed. 53 (2014) 10485–10489.
[48] J.C. Yu, J. Yu, W. Ho, Z. Jiang, L. Zhang, Chem. Mater. 33 (2002) 3808–3816.
[49] J. Georgieva, S. Armyanov, E. Valova, I. Poulios, S. Sotiropoulos, Electrochem. Commun. 9 (2007) 365–370.
[50] J.H. Kim, F. Nishimura, S. Yonezawa, M. Takashima, J. Fluorine Chem. 144 (2012) 165–170.
[51] S.G. Yang, S. Cheng, X.Y. Li, Z.Q. Gong, Q. Xie, J. Hazard. Mater. 175 (2010) 258–266.
[52] S. Boobas, J. Jayaprakash, R. Ranjith, A. Priyadharsan, V. Krishnakumar, Ionics 25 (2018) 1–12.
[53] M. Qamar, Q. Drmosh, M.I. Ahmed, M. Qamaruddin, Z.H. Yamani, Nanoscale Res. Let. 10 (2015) 1–6.
[54] J.Y. Cheng, J. Chen, W. Lin, Y.D. Liu, Y. Kong, Appl. Surf. Sci. 332 (2015) 573–580.
[55] E.M. Samsudin, S.B.A. Hamid, J.C. Juan, W.J. Basirun, A.E. Kandjani, S.K. Bhargava, Appl. Surf. Sci. 365 (2016) 57–68.